Phosphorylation-induced flexibility of proto-oncogenic Bcl3 regulates transcriptional activation by NF-κB p52 homodimer

Wenfei Pan[1,5], Tapan Biswas[2,5], Shandy Shahabi[2], William Suryajaya[2], Andres Vasquez[2], Qian Du[2], Gourisankar Ghosh[2,6] & Vivien Ya-fan Wang[1,3,4,6]

[1]Faculty of Health Sciences, University of Macau, Avenida da Universidade, Taipa, Macau SAR, China
[2]Department of Chemistry and Biochemistry, University of California, San Diego, 9500 Gilman Drive, La Jolla, CA 92093, USA
[3]Cancer Centre, Faculty of Health Sciences, University of Macau, Avenida da Universidade, Taipa, Macau SAR, China
[4]MoE Frontiers Science Center for Precision Oncology, University of Macau, Avenida da Universidade, Taipa, Macau SAR, China
[5]equal contributions
[6]co-corresponding authors: Email: gghosh@ucsd.edu and vivienwang@um.edu.mo

Keywords: Bcl3, NF-κB p52:p52 homodimer, transcriptional regulation, conformational dynamics, HDX-MS

Abstract

The overexpression of proto-oncogenic protein Bcl3 is observed in various cancers. Bcl3 is extensively phosphorylated and associates with NF-κB p50 and p52 homodimers to regulate transcription. Through cellular and biochemical assays, we observed that phospho-mimetic Glu substitution of Bcl3 Ser366 in addition to previously studied Ser33, 114 and 446 is necessary to switch it from an IκB-like inhibitor to a transcriptional activator. To study interactive features of p52 homodimer and Bcl3, and phospho-modification mediated changes in Bcl3 that regulates DNA-binding by p52, we performed HDX-MS of both Bcl3 and p52 within various complexes. Nature of interactions within Bcl3:(p52:p52) complex in presence and absence of DNA, and differential flexibility and allosteric changes in Bcl3 upon phospho-modifications revealed why a facile accommodation of DNA requires phosphorylations. The inhibitory nature of unphosphorylated Bcl3:(p52:p52) complex for DNA binding was also relieved by deletion of Bcl3 C-terminal 28 residues. Overall, this study revealed mechanistic bases of how phospho-modification of Bcl3 regulate transcriptional potential of NF-κB and intricate cell physiology, a dysregulation of which can lead to cancers.

Introduction

B-cell lymphoma 3 (Bcl3) was initially discovered due to its constitutive expression in many B cell cancers (Ohno et al. 1993), and later observed to be highly expressed in various cancers, including solid tumors, due to either aberrant chromosomal translocation of the gene or over expression without chromosomal rearrangement (Nishikori et al. 2003; Mathas et al. 2005; Maldonado and Melendez-Zajgla 2011). Bcl3 belongs to the inhibitor of the NF-κB (IκB) family of proteins that regulate the transcriptional activities of the NF-κB family of transcription factors. Three classical members of the IκB family (IκBα, -β and -ε) form binary complexes with homo- and hetero-dimers of RelA and cRel of the NF-κB family in the cytoplasm to prevent their access to and association with DNA in the nucleus, thereby inhibiting their transcriptional activities (Huxford, Hoffmann, and Ghosh 2011; Basak et al. 2007). In contrast, Bcl3 associates with the p52:p52 and p50:p50 homodimers of NF-κB family in the nucleus (Bours et al. 1993; Fujita et al. 1993; Inoue et al. 1993). Bcl3 associates with pre-formed p50 homodimer in cells (Pan et al. 2022) and induces formation of p52 homodimer although the heterodimeric complexes of p52 with RelA, RelB and cRel are preferred. IκBζ, another IκB family protein, functions similarly to Bcl3 as transcriptional coregulator by preferentially associating with the p50:p50 homodimer in the nucleus (Trinh et al. 2008; Bates and Miyamoto 2004; Yamamoto et al. 2004; Kohda, Yamazaki, and Sumimoto 2016).

The biological function of Bcl3 is diverse; however, its most notable function is the induction of cell proliferation by activating the expression of cyclin D1 (Cogswell et al. 2000; Westerheide et al. 2001). Bcl3 also facilitates the development of splenic B cells, the expansion and recall response of memory T cells, and the priming of CD4 and CD8 cells by dendrites (Franzoso et al. 1997; Schwarz et al. 1997). Deletion of the Bcl3 gene does not show any overt phenotype in cells; however, it causes poor immune response when these cells are challenged with infection. This observation tallies with a protective function of the lack of Bcl3 in autoimmune diseases such as colitis and experimental autoimmune encephalomyelitis (EAE) (Liu et al. 2022). The mechanism underlying function of Bcl3 as a transcriptional coregulator or its preference for only two specific NF-κB dimers, (p52:p52 and p50:p50 homodimers), is unclear. Tissue-specific variation in expressions of p50 and p52, and their alternative production mechanisms suggest that functions of Bcl3 is likely to be cell type- and signal-specific.

The structural organization of Bcl3 is similar to other IκB proteins, containing a centrally folded ankyrin repeat domain (ARD) flanked by flexible N- and C-terminal regions (Figure 1A-1B). Prototypical IκB proteins (IκBα, -β and -ε) are rarely involved in transcriptional activity in the nucleus. Rather, their ubiquitination and proteosome-mediated degradation upon phosphorylation at the N-termini by signal-induced IκB kinase (IKK) leads to nuclear transport of NF-κB dimers and transcriptional activation. Bcl3 is not reported to have such phosphorylation sites regulating its degradation. Instead, phosphorylation of serine at position 33 (S33) at the N-terminal region of Bcl3 is critical for its nuclear localization, and consequent protection from constitutive cytoplasmic degradation (Wang et al. 2017). Bcl3, IκBα, and IκBβ all contain proline and serine rich (PEST) sequences in their C-termini. Phosphorylation at the PEST

sequence in IκBα renders it a stronger inhibitor (Phelps et al. 2000) but modification of these serines to asparagine render a transcriptional coactivator function to IκBα (Dembinski et al. 2017). In contrast, Bcl3 is heavily phosphorylated at its C-terminal serine and threonine residues in cell, some of the phosphorylations being critical for transcriptional activation (Wang et al. 2017). The primary focus of this study is to clarify mechanisms underlying the phosphorylation-mediated transcriptional coregulatory functions of Bcl3.

The *E. coli* or baculovirus expressed Bcl3 (presumably unphosphorylated) fails to form a ternary complex with (p52:p52):DNA (Nolan et al. 1993); rather it expels DNA from p52 to form a stable Bcl3:(p52:p52) binary complex. A structural model of the Bcl3:(p52:p52):DNA ternary complex, predicted from structural knowledge of similar subcomplexes, indicates a clash of the C-terminal region and PEST sequence of Bcl3 with the negatively charged DNA (Figure 1E-1F). This agrees with the stripping of DNA from homodimers of p50 and p52 by unphosphorylated Bcl3 (Nolan et al. 1993) (Figure 1H, lanes 6-7). This stripping effect of Bcl3, which reflects its functional resemblance to inhibitory IκBα, is not yet reported in cells. Earlier, we observed that phosphorylation at S33 of Bcl3 is required for its nuclear localization, and that at S114 and S446 for the formation of the Bcl3:(p52:p52):DNA ternary complex (Wang et al. 2017). S114 is located within the flexible N-terminal region just next to the ARD, and S446 is the C-terminal residue of Bcl3. Mutation of S114 and S446 of Bcl3 to alanine abolished cyclin D1 expression and inhibited the migratory function of U2OS cells. However, if expressed and isolated from mammalian cells, this mutant protein could still form a ternary complex with p52 and DNA (Wang et al. 2017). This hints at more complex possibilities through various post-translational modifications of Bcl3 at other site(s), some of which will enable Bcl3 to form a ternary complex, and perhaps trigger transcriptional activation of specific genes.

In this study, we observed phosphorylation of Bcl3 additionally at residue S366 in promoting formation of a stable ternary complex, and transcriptional activation of genes in cells. To probe effect of phosphorylation, especially at its C-terminal region, on structural properties of Bcl3 that help stabilize the Bcl3:p52:DNA ternary complex for regulation of transcriptional activation, we performed hydrogen-deuterium exchange mass spectrometry (HDX-MS) analyses on both Bcl3 and p52. The deuterium uptakes of p52 and both wild-type Bcl3 (Bcl3-WT) and its phospho-mimetic version containing S33E, S114E, S366E, and S446E substitutions (Bcl3-4E) were measured in various (sub)complexes of p52:p52 homodimer with cognate κB-DNA and Bcl3. This revealed interactive features of p52 and Bcl3, and in particular underscored phosphorylation-related changes in flexibility of Bcl3 that allowed extrusion of the CTD of Bcl3 from the DNA-binding interface of p52 for accommodation of cognate DNA. These along with data of cellular experiments reveal role of phosphorylation in transcriptional coactivator function to Bcl3. A truncation of the C-terminal 28-residues of Bcl3 recapitulated phosphorylation mediated changes in function for Bcl3 and provided experimental proof to the conclusion from HDX data. The presence of several oncogenic mutations including frameshifts located within the CTD (COSMIC database,

https://cancer.sanger.ac.uk/cosmic/gene/analysis?ln=BCL3) (Forbes et al. 2015) of Bcl3 highlight its importance in transcriptional regulation.

Results

Phosphorylation of S366 in Bcl3 is essential for its association with the promoter and transcriptional activation

We set out to determine if other phosphorylation, in addition to phosphorylation at S33, S114 and S446 of Bcl3 could enhance its ability to associate with the (p52:p52):DNA binary complex and induce gene activation. Examination of mass-spectrometry data from our previous experiments and publicly available proteomic databases of different cancer cells identified new phosphorylation sites that have not been studied. We identified phosphorylation at S366 in our sample and observed that it is common in cancer cells. S366 is located at the C-terminal flexible region of human Bcl3 which is in the vicinity of the DNA-binding interface of p52 in the ternary complex model (Figure 1E-1F). Hence, we investigated if phosphorylation at S366 could play a regulatory role. Bcl3 is constitutively phosphorylated when over-expressed in cells. Therefore, phospho-inactive S336A and phosphor-mimetic S366E mutants were generated to study the effect of phosphorylation at S366. Using a reporter gene expression assay, we observed a reduction in p52-dependent transcriptional activation upon S366A substitution of Bcl3, whereas a slight enhancement upon S366E substitution comparing to the constitutive phosphorylated wild-type (WT) Bcl3 (Figure 1G). The difference in transcriptional output between these two mutants is the result of the state of phosphorylation of S366, although it is important to note that these phospho-inactive and phospho-mimetic Bcl3-S366A and Bcl3-S366E proteins are likely to have undergone common phospho-modifications at other sites such as at S33, S114 and S446, in cells.

To test the effect of the S366E modification on the stability of the Bcl3:(p52:p52):DNA ternary complex, we performed EMSA assays with WT Bcl3 and its multiple variants using bacterial recombinant proteins which allow us to specifically access the effect on these mutants since no other sites are subjected to modification in bacteria (Figure 1H). The ternary complex formed with Bcl3-4E was stable at a higher concentration. The co-elution of Bcl3-4E, p52, and DNA observed in size-exclusion chromatography further supports the increased stability of the Bcl3-4E:(p52:p52):DNA ternary complex (Figure S1).

Impact of phosphorylation on Bcl3 dynamics in absence of p52

Structural information about the flexible N- and C-terminal regions where phosphorylatable residues (S33, S114, S366 and S446) under study here is lacking likely due to their flexible nature (Figure 1A-1B). To explore the dynamics of the N-terminal (1-125), ARD (126-362), and C-terminal (363-446) regions and interactions among them, we performed HDX-MS (Ramirez-Sarmiento and Komives 2018; Vinciauskaite and Masson 2022; Oganesyan, Lento, and Wilson 2018) analyses to measure deuterium uptakes at 0.5-, 1-, 2-, and 5-minute timepoint on Bcl3-WT and Bcl3-4E as free proteins (Figure 2A-2C). For free Bcl3-WT, 107 distinct peptides were identified with an average redundancy of 4.04, and this rendered a coverage of

98% with only two short segments spanning residues 1-6 and 249-251 missing. For Bcl3-4E, a total of 88 distinct peptides were identified with an average redundancy of 3.16, rendering a coverage of 99% with only a small segment spanning residues 249-251 missing. Deuterium uptake plots reveal the most significant difference between these two molecules lies in the 9-45 peptide (Figure 2G). The uptake is negligeable in Bcl3-4E compared to Bcl3-WT suggesting this region in Bcl3-4E is rigid. This segment contains S33E which is known to stabilize Bcl3 from degradation by preventing the binding of ubiquitin E3 ligase TBLR1 (Keutgens et al. 2010). The structural stability of this segment explains why TBLR1 fails to bind the S33 phosphorylated Bcl3 allowing it to move to the nucleus for its transcriptional activity.

Except for the 9-45 region, the uptake pattern is highly similar between the two proteins. However, the extent of protection is higher in Bcl3-WT (exchanged less) than Bcl3-4E (Figure 2A). The N- and C-terminal regions of both proteins displayed high exchange, suggesting their significant flexibility; however, a peptide encompassing residues 9-45 is more resistant to exchange in Bcl3-4E compared to Bcl3-WT as mentioned above. Since S33E substitution is located within this segment, local structural change induced by S33E most likely results in this resistance. The exchange propensity of individual ankyrin repeats (ARs) in the ARD displayed striking variability for Bcl3-WT and Bcl3-4E. As anticipated for a folded domain, AR1-5 is resistant to exchange with AR2 and AR3 manifesting the highest resistance (Figure 2D). However, the deuterium uptakes of AR6 and AR7 are noticeably higher, indicating their flexibility and reflecting their structural adaptability to accommodate DNA (Figure 2F). Noticeably, stretches of both AR1 (141-148) and AR7 (329-339) (Figure 2A, 2E) were significantly more flexible in Bcl3-4E than Bcl3-WT. It is possible that substitutions of S114E and S366E in nearby regions led to these effects in AR1 and AR7 of Bcl3-4E, respectively. Overall, these HDX-MS data on exchange propensity reveal that barring a segment within the N-terminal region surrounding S33E which is more rigid, the rest of Bcl3-4E is more flexible than Bcl3-WT, suggesting a role of phospho-mimetic substitutions in regulating the activity of Bcl3 through dynamism.

Dynamics of p52 in the absence of DNA

To observe dynamics of p52 in its homo-dimeric complex, we performed HDX-MS analyses to measure deuterium uptakes at 0.5-, 1-, 2-, and 5-minute timepoints on p52 within its dimer (Figure 3). As anticipated, the N-terminal region (1-34) and the C-terminal GRR region (354-398) exchanged rapidly suggesting their flexibility. The NTD showed mixed properties, with some areas exchanging rapidly and some highly resistant (Figure 3C-3E). The DD was observed to be rather resistant to exchange, indicating its stabler fold (Figure 3A). In addition, we also measured the uptakes of p52 homodimer in the presence of its target DNA and/or Bcl3. The exchange propensity of various regions changed upon binding to DNA and/or Bcl3. These changes are described in detail in a later section.

Changes in dynamics of Bcl3 within Bcl3:(p52:p52) binary complex and Bcl3:(p52:p52):DNA ternary complex

We further performed HDX-MS studies of the p52 homodimer bound to Bcl3-WT and Bcl3-4E to understand how phospho-mimetic mutations of Bcl3 alter its binding dynamics with p52. We also performed this study using Bcl3-4E bound to both p52 homodimer as a binary complex and (p52:p52):DNA as a ternary complex to better understand how the phospho-mimetic changes help accommodate DNA. The HDX-MS data indicated unique dynamism in Bcl3 upon its binding to p52 homodimer or (p52:p52):DNA complex. One of the striking features of these complexes is that the differences in exchange between free Bcl3 and p52-bound Bcl3 are very similar in both Bcl3-WT vs. -4E binary complexes where they showed similar exchange patterns (protection or exposure), but Bcl3-4E is more dynamic both in free and p52-bound states (Figure 4A). That is, Bcl3-WT is more protected (exchanged less) than Bcl3-4E in both states (Figure 4F-4G, 4I-4J and Figure S4). In addition to uptake plots of Bcl3 in the complexes, we also plotted differences in exchanges in the binary complexes of the two Bcl3 proteins (Bcl3-WT:(p52:p52) vs. Bcl3-WT, and Bcl3-4E:(p52:p52) vs. Bcl3-4E) which show the relative effect of p52 on these two Bcl3 proteins (Figure 4B-4C). As indicated earlier, the N-terminal 9-45 region is protected in free Bcl3-4E (Figure 2A and 2G) but exposed in the binary complex with p52 (Figure 4C and 4E); however, the dynamicity of this region in Bcl3-4E changes further significantly from free in Bcl3:(p52:p52) binary complex to rigid in Bcl3:(p52:p52):DNA ternary complex (Figure 4D). The corresponding region in Bcl3-WT does not change upon binding to p52 (Figure 4B). The rest of the N-terminal region in Bcl3-WT, residues 46-115, showed no significant difference in exchange in free and p52-bound states. This corresponding segment in Bcl3-4E is slightly more protected in the Bcl3-4E:(p52:p52) binary complex than in free Bcl3. Most of AR1 (120-159) was protected in both binary complexes; the entire AR2-4 (160-265) is slightly exposed in both binary complexes; and the last three ARs (AR5-7, 267-362) are more protected in both cases. The C-terminal region of Bcl3-WT do not show many changes, while Bcl3-4E is slightly protected by p52 (Figure 4B-4C).

There are no major changes in the uptake plots of Bcl3-4E in the Bcl3-4E:(p52:p52):DNA ternary complex compared to the Bcl3-4E:(p52:p52) binary complex barring the N-terminal 9-45 region (Figure 4D). Structural transition of 9-45 region from rigid in free, to flexible in binary complex and back to rigid in the ternary complex is intriguing. The DNA-induced structural stability is allosteric in nature which might facilitate recruitment of selective factor for transcription regulation. However, barring this segment, the difference uptake plot (Bcl3-4E:p52:DNA – Bcl3-4E:p52), which accounts for the impact of DNA on the Bcl3-4E:p52 binary complex, showed small alterations throughout the Bcl3-4E protein. Moving along the molecule from 9-45 towards the C-terminus reveals that regions showing protection (60-115 and 320-446) in the binary complex are deprotected in the ternary complex and the region showing deprotection (120-265) is protected in the ternary complex (Figure 4C-4D). The segment 265-320 showed less protection in the ternary complex compared to the binary complex. The uptake plots of the C-terminal segment of Bcl3-4E (425-446) in its free form and as a ternary complex are comparable, whereas it is protected in the binary complex with p52 (Figure 4K). Since the C-terminus positions close to the DNA binding region of p52

interfering with DNA binding, higher exchange of the C-terminus in the ternary complex suggests its exclusion from the DNA binding surface.

Changes in dynamics of p52 within the (p52:p52):DNA and Bcl3:(p52:p52) binary complexes and Bcl3:(p52:p52):DNA ternary complex

To understand the altered dynamics of p52 as it transits from a free dimeric protein to a binary complex with Bcl3-4E and a ternary complex with Bcl3-4E and DNA, we compared deuterium uptakes of p52 within these complexes. Bcl3 interacts asymmetrically with two identical protomers of p52 within its homodimer, similar to the binding mode observed for the interaction of IκBα with the p50:RelA heterodimer (Ramsey et al. 2017; Huxford et al. 1998) (Figure 1E-1F). Thus, the protection or deprotection maps observed reflect an average of two specific interaction patterns. p52 binds DNA using five loops (L): L1 (45-78), L2 (140-145), L3 (220-229), L4 (251-258) and L5 (274-279) (PDB 1A3Q and 7CLI) (Cramer et al. 1997; Pan et al. 2023). The DNA binding protects p52 from deuterium uptake in three large regions: 30-90, 150-190 and 230-310 (Figure 5A, 5E and 5F). In each of these regions, some segments were more protected than others, and some show no change. The DNA contacting residues in loops L2 and L3 appeared to be unprotected. Residues emanating from these two loops contact the center of DNA asymmetrically; loop L2 or L3 from one subunit of the dimer is stable and the other is flexible. In HDX-MS experiments of the (p50:RelA):DNA complex, these loops of the RelA subunit appeared unprotected, while the corresponding loops in p50 were protected (Narang et al. 2018). We suggest that the appearance of a lack for protection of these loops in the p52:DNA complex might be a result of asymmetric binding. Interestingly, DNA protects only a limited number of peptides of p52 in the binary complex, and a few of these are the DNA binding loops L1, L4 and L5. A segment within the glycine rich regions (GRR) of p52 (377-382), which is located away from the DNA binding surface, is deprotected upon DNA binding (Figure 5G), similar to that observed in the case of p50 C-terminus in the (p50:RelA):DNA complex.

Bcl3-4E protects the entire p52, barring a few short segments (residues 90-120, 170-180, 190-200 and 275-280) (Figure 5B). The protected regions include the DNA binding loops L1-L5. Protection of these loops, in particular, the 30-90 region, which contains the sequence specific DNA binding loop L1 region by Bcl3-4E, poses a challenging concern as to how DNA binding is maintained in the Bcl3-4E:(p52:p52):DNA ternary complex. Only some regions protected by Bcl3-4E in the binary complexes remained protected in the ternary complex (compare Figure 5B and 5D). Only two peptides, residues 229-248 (Figure 5H) and residues 289-306 (Figure S3), show enhanced protection in the ternary complex as compared to that in the binary complexes. Of these, 229-248 contains loop L3 which is engaged in DNA binding.

The differential protection map reveals that while the presence of Bcl3-4E in the ternary complex renders p52 globally more dynamic (Figure 5A-5D), this complex possesses certain features alluding to its unique ternary complex formation property. Indeed, the p52 protection map in the ternary complex showed that the DNA binding loops within the NTD were mostly exposed, suggesting that DNA binding might occur

transiently. The greatest protection is observed in p52 DD, residues 289-306 (Figure 5C-5D and Figure S3). This segment was not protected by Bcl3-4E and was only partially protected by DNA in the binary complexes (Figure 5A-5B). A segment in p52 NTD, residues 85-95, showed deprotection in both binary complexes, and the deprotection was lost in the ternary complex (Figure 5B-5C). This suggests that Bcl3 reorganizes p52's interactions with DNA in its NTD, likely antagonizing binding of p52 to DNA. When p52 is bound to DNA, the effect of Bcl3-4E on p52 is largely similar with a couple of striking differences (Figure 5D); Bcl3-4E enhanced deprotection of p52 NTD residues 152-168, and it reduced protection of residues 275-285 which is located within p52 DD and close to the DNA-binding interface. The protection of 289-307 region remained similar upon Bcl3-4E binding.

The mechanism of phosphorylation-mediated transcriptional regulatory switch of Bcl3

The HDX data suggests that phosphorylation of S366 and S446 triggers altered conformation of the flexible C-terminal region of Bcl3 (Figure 2), with apparent loss of several contacts with the DNA binding NTD of p52. It is possible that some of this loss in interactions is partly compensated for by new contacts, possibly between the ARD of Bcl3 and the βe-βf loop (289-306) within the p52 DD (Figure 5C-D, Figure S3). This segment in the NF-κB family members is unique (Figure 6A), suggesting such contacts to be NF-κB subunit specific. A structural model of the Bcl3:(p52:p52) complex indicates that the βe-βf loop is located near the AR3 of Bcl3, suggesting the possibility of contacts between the two proteins via this loop. To test this, we replaced the βe-βf loop sequence of p52 with counterparts from p50 (named p52-KDIN) and RelA (named p52-ADPS) and performed a pulldown experiment using biotinylated P-Selectin-κB DNA with equal amounts of p52-WT or mutant p52 (p52-ADPS and p52-KDIN) alone, Bcl3-4E alone, or a mixture with p52-WT, p52-ADPS or p52-KDIN mutants (Figure 6B). We found that the p52-KDIN mutant retained lesser amounts of Bcl3-4E compared to p52-WT. However, the p52-ADPS mutant showed no significant difference. Although this p52-ADPS mutant appeared to bind the DNA better than p52-WT in the absence of Bcl3-4E. We further tested if these mutants were less effective in driving transcription. We observed significantly reduced transcriptional activity of both of these p52 mutant proteins in a reporter-based assay (Figure 6C). These results suggest that the βe-βf loop of p52 plays a role in transcription, likely through its involvement in Bcl3 binding to drive transcription. These results also hint at the possibility of Bcl3 acting as an allosteric regulator of p52, dictating the nature of the molecular interaction between p52 and DNA.

Furthermore, the changes in deuterium uptake properties of both Bcl3 and p52 strongly suggest that the C-terminal flexible region of Bcl3 is juxtaposed with the p52 NTD and makes direct contacts, which results in the inhibition of DNA binding by p52. Phosphorylation of Bcl3 at S366 and S446 alleviates this inhibitory effect on DNA binding by p52. This prompted us to test if deletion of the C-terminal segment of Bcl3 could relieve its inhibitory activity towards forming a ternary complex. We generated a truncation mutant of Bcl3-WT lacking 28 C-terminal residues (Bcl3-WT$^{1-418}$) (Figure 6D). The luciferase reporter assay with co-expression of Bcl3-WT$^{1-418}$ together with p52 showed higher luciferase activity compared to Bcl3-

WT in cells. It should be noted that unlike the unphosphorylated recombinant Bcl3-WT protein in *E. coli*, Bcl3-WT is phosphorylated when transfected in cells and able to induce reporter expression. However, phosphorylation may not be 100% at S366 and S446, resulting in mixed results. The removal of Bcl3 C-terminal tail abrogates its inhibitory effect, irrespective of the phosphorylation state of S366. Together, these results support our hypothesis that the C-terminal region of Bcl3 is detrimental to ternary complex formation. Phosphorylation of both S366 and S446 likely renders structural alteration and likely increased flexibility of the C-terminal region of Bcl3, thereby allowing the access of p52 to target DNA while p52 remains bound to Bcl3 and allowing its transcriptional coactivator function (Figure 6E).

Discussion

This study explores how Bcl3, a member of the IκB family of proteins, functions as a regulator of p52-mediated transcriptional activation. It has long been known that Bcl3 requires phosphorylation to function as a transcriptional coactivator (Bundy and McKeithan 1997). In this study, we show that phosphorylation at four sites, two at the N- and two at the C-terminal flexible regions, is necessary for the transcriptionally competent Bcl3:(p52:p52):DNA ternary complex formation. Several other residues also undergo phosphorylation and their roles in transcription have not been exhaustively investigated. Barring phosphorylation of S33, which is essential for the stabilization and nuclear localization of Bcl3, it is not clear if phosphorylation of any of the other three sites is strictly required for all transcription events mediated by the Bcl3:(p52:p52) complex. It is possible that combinatorial phosphorylation induces gene-specific transcription. Our study reveals that the C-terminal 20-30 residues of Bcl3 are inhibitory to ternary complex formation. Phosphorylation of both S366 and S446 moves the C-terminal tail of Bcl3 away from the (p52:p52):DNA interface. The mutations of S366 had been previously described in cancers or inflammatory diseases (COSMIC database legacy identifier number COSM9762159 and COSM10046017) (Bonilla et al. 2016; Yuan et al. 2016), suggesting its significance in switching Bcl3's activity. This does not suggest, but is possible, that S366 and S446 phosphorylation occur only under pathogenic conditions. Further studies are required to determine if different sets of phosphorylation within the C-terminal flexible region are needed for Bcl3's transcriptional activity under pathogenic and non-pathogenic conditions.

Results shown here reveal that phosphorylation of Bcl3 makes it more dynamic, with more uptake throughout the molecule except for its N-terminal 9-45 region. Surprisingly, dynamism persists even when it binds to p52 homodimer and to the (p52:p52):DNA complex. Very little new contacts between p52 and DNA are formed when Bcl3-4E binds to the (p52:p52):DNA complex. Instead, most of the specific and high energy contacts between p52 and DNA are lost, suggesting that Bcl3-4E weakens the (p52:p52):DNA complex. It is possible that specific protein factors assemble into this ternary complex to enhance the stability of the multiprotein transcriptional complex. Our study also reveals that the dynamism of Bcl3 9-45 region alters from its free to (p52:p52)-bound or to the (p52:p52):DNA-bound states. In the ternary complex, this region is less exposed, suggesting the DNA induces an allosteric conformational change.

This region has also been shown to recruit ubiquitin ligase in the cytoplasm only when S33 remains unmodified, suggesting that the DNA-induced conformational change of this region may play an important role in recruiting different factors in the nucleus. In this study, we used a natural G/C-centric P-Selectin-κB DNA, which is known to recruit histone acetylases to the Bcl3:(p52:p52) complex, activating transcription. In contrast, an A/T-centric κB DNA, which represses transcription by recruiting histone deacetylase, might alter the conformation of this region differently when it binds to the Bcl3:(p52:p52) binary complex. Such changes could facilitate recruitment of histone deacetylases. Future experiments will clarify if that the case.

Bcl3 is an oncoprotein, which has been implicated in a wide range of cancers, both hematological and solid tumors. The constitutive nuclear presence of Bcl3 induces chronic inflammation and proliferation by maintaining high levels of cyclin D1 and inflammatory cytokines, controlling both tumor growth and proliferation. In the vast majority of cases where aberrant Bcl3 is responsible for the cancer phenotype, it is overexpressed. Bcl3 is also mutated in several cases. Although the effect of these mutations has not been investigated, a significant number of these mutations, including frameshift mutations, are clustered in its C-terminal regions (COSMIC database). Our results clearly suggest that the C-terminal deletion of Bcl3 would activate genes responsible for inflammatory and proliferative genes.

Materials and Methods

Protein Expression and Purification

Recombinant non-tagged human p52 (1-398)-WT, -ADPS and -KDIN mutants were expressed and purified from *Escherichia coli* Rosetta (DE3) cells. Rosetta (DE3) cells transformed with pET-11a-p52 (1-398)-WT, -ADPS or -KDIN mutants were cultured in 2 L of LB medium containing 50 mg/mL ampicillin and 34 mg/mL chloramphenicol at 37 ^{o}C. Expression was induced with 0.2mM Isopropyl β-D-1-thiogalactopyranoside (IPTG) at OD_{600} 0.5-0.6 for 3 hours. Cells were harvested by centrifugation, suspended in 40 mM Tris-HCl pH 7.5, 100 mM NaCl, 10 mM β-Mercaptoethanol (β-ME), 1 mM PMSF, and lysed by sonication. Cell debris was removed by centrifugation (20,000 g for 30 min). Clarified supernatant was loaded onto Q-Sepharose FF column (GE Healthcare). Flow-through fraction was applied to SP HP column (GE Healthcare). The column was washed with 40 mM Tris-HCl pH 7.5, 200 mM NaCl; 10 mM β-ME, and the protein was eluted by the same buffer containing 400 mM NaCl. p52 was concentrated and loaded onto the gel filtration column (HiLoad 16/600 Superdex 200 pg, GE Healthcare) pre-equilibrated with 10 mM Tris-HCl (pH 7.5), 100 mM NaCl; 5 mM β-ME. Peak fractions were concentrated to ~10 mg/mL, flash frozen in liquid nitrogen and stored at -80°C.

Recombinant human His-Bcl3 (1-446)-WT, phospho-mimetic mutants, and (1-418) C-terminal deletion mutant were expressed in *Escherichia coli* Rosetta (DE3) cells by induction with 0.2 mM IPTG at OD_{600} 0.4 for 8 hours at 24°C. Cell pellets of 2 L-culture of Bcl3 alone or together with 1 L-culture of p52 (for p52:p52:Bcl3 complex) were resuspended together in buffer containing 20 mM Tris-HCl pH 8.0, 300 mM

NaCl, 25 mM imidazole, 10% (v/v) glycerol, 10 mM β-ME, 0.1 mM PMSF and 50μL protease inhibitor cocktail (Sigma, Cat#P8465) and then purified by Ni Sepharose (HisTrap HP, GE) followed by anion exchange column (Q Sepharose fast flow, GE). The protein complexes further went through HiTrap Desalting Column (GE) to exchange buffer before other assays.

Luciferase Reporter Assays

HeLa cells were obtained from ATCC (CCL-2) and cultured in Dulbecco's modified Eagle's medium (DMEM; Gibco, Cat#11995065) that was supplemented with 10% fetal bovine serum (FBS; Gibco, Cat#10270106) and 1x Penicillin-Streptomycin-L-Glutamine (Corning, Cat#30-009-CI). HeLa cells were transiently transfected with Flag-p52(1-415)-WT (or various mutants) together with Flag-Bcl3(1-446) (or various mutants) expression vectors or empty Flag-vector, and the luciferase reporter DNA with P-Sel-κB DNA promoter (Wang et al. 2012). The total amount of plasmid DNA was kept constant for all assays. Transient transfections were carried out using polyethylenimine (PEI) (Polysciences, Cat#23966). Cells were collected 48 hours after transfection. Luciferase activity assays were performed using Dual-Luciferase Reporter Assay System (Promega, Cat#E1910) following the manufacturer's protocol. Data are represented as mean standard deviations (SD) of three independent experiments in triplicates.

Electrophoretic Mobility Shift Assays (EMSA)

The oligonucleotides containing κB site (Wang et al., 2012) used for EMSA were PAGE purified, end radiolabeled with ^{32}P using T4-polynucleotide kinase (NEB, Cat#M0201) and [γ-^{32}P] ATP, and annealed to the complementary strands. Binding reaction mixtures contained indicated recombinant proteins or nuclear extracts at different concentrations, binding buffer (10mM Tris-HCl pH 7.5, 50mM NaCl, 10% (v/v) glycerol, 1% (v/v) NP-40, 1mM EDTA, 0.1mg/mL poly(dI-dC)), and ~10000cpm of ^{32}P-labeled DNA. Reaction mixtures were incubated at room temperature for 20 minutes and analyzed by electrophoresis on a 5% (w/v) non-denatured polyacrylamide gel at 200V for 1 hour in 25mM Tris, 190mM glycine, and 1mM EDTA. The gels were then dried, exposed to a phosphorimager, and scanned by Typhoon scanner 9400 (Amershan Bioscience). Gels were quantified by using ImageQuant version5.2 (Molecular Dynamics).

Streptavidin Pulldown Assays

100 nM annealed biotinylated P-Selectin-κB DNA was pre-incubated with 15 μL streptavidin magnetic beads (MedChemExpress, Cat#HY-K0208) using incubation buffer containing 10 mM Tris pH 7.5, 1 mM EDTA, 1 M NaCl, 0.02% (v/v) Tween-20 at 4°C for 1 hour followed by washing with 1 mL incubation buffer. 80 ng of recombinant non-tagged p52(1-398)-WT or -ADPS, -KDIN mutant protein were mixed with recombinant 0.8 μg His-Bcl3(1-446)-4E protein in binding buffer containing 20 mM Tris pH 7.5, 100 mM NaCl, 0.1% (v/v) NP-40, and 1 mM DTT. Complexes of p52 with His-Bcl3-4E were then pull-downed using 15 μL Biotin-κB DNA pre-incubated streptavidin magnetic beads at 4°C for 2 hours. Bound complexes were washed three times with binding buffer and dissolved in 4xSDS-dye by boiling at 95°C for 10 minutes

followed by SDS-PAGE. Bound p52 and His-Bcl3-4E proteins were visualized by immunoblotting using anti-NF-κB p100/p52 antibody (Cell Signaling Technology, Cat#4882) and anti-His antibody (Bio Bharati Life Science, Cat#BB-AB0010) respectively. The pulldown assays were performed in triplicate, immunoblotting images were then analyzed using Image-J software to measure the band intensity of p52 and Bcl3-4E.

Hydrogen-Deuterium Exchange Mass Spectrometry (HDX-MS)

Bcl3-WT or Bcl3-4E and p52 (i.e., p52:p52 homodimer) were exchanged to HDX buffer (300 mM NaCl, 25 mM Tris pH 8.0, 5 % glycerol, 10 mM β-mercaptoethanol) prior to HDX-MS experiments. Commonly, a 100 µL volume of concentrated protein was loaded onto a Superose6 5/150 increase column (Cytiva), and appropriate elution peak fractions from multiple runs were combined and concentrated using a protein concentrator (Sartorius, Vivaspin, 30,000 MWCO) to obtain a final sample of ~300 µL at ~30 µM concentration.

For HDX-MS of Bcl3 and p52 homodimer, proteins at 10 µM concentration in HDX buffer were used. When HDX-MS of IKK2 and NEMO were performed in the presence of Ub_4, a three-fold molar excess of Ub_4 (i.e., ~30 µM) was present.

For HDX-MS of Bcl3:(p52:p52) complex, an equimolar mixture of Bcl3 and p52 homodimer was HDX-buffer exchanged using a Superose 6 5/150 increase column. Peak fractions of the Bcl3:(p52:p52) complex from multiple runs were pooled and concentrated, and the concentration was adjusted to ~5 µM. When HDX-MS assays of Bcl3:(p52:p52) was performed in presence of Ub_4, the concentration of Bcl3:(p52:p52) complex was ~3 µM and that of Ub_4 was ~9 µM.

HDX-MS was performed at the Biomolecular and Proteomics Mass Spectrometry Facility (BPMSF) of the University California San Diego, using a Waters Synapt G2Si system with HDX technology (Waters Corporation) as described previously (Ramirez-Sarmiento and Komives 2018; Vinciauskaite and Masson 2022). Deuterium exchange reactions were performed using a Leap HDX PAL autosampler (Leap Technologies, Carrboro, NC). The HDX-buffer for deuteration contained 300 mM NaCl, 25 mM Tris pH 8.0, 5% glycerol, and 10 mM β-mercaptoethanol in D_2O. D_2O was exchanged for H_2O by lyophilizing buffers initially prepared in ultrapure water and redissolving in the same volume of 99.96% D_2O (Cambridge Isotope Laboratories, Inc., Andover, MA) immediately before use. Measurements were made in triplicate for each deuteration timepoint analyzed (0.5, 1, 2, and 5 min). For each reaction, a 4 µL volume of sample (at the abovementioned concentrations) was stabilized at 25°C for 5 min prior to mixing with 56 µL of D_2O containing HDX-buffer. The reaction was quenched for 1 min at 1°C by combining 50 µL of the reaction with 50 µL of 3 M guanidine hydrochloride, final pH 2.66. The quenched sample (90 µL) was then injected in a 100 µL sample loop, followed by digestion on an in-line pepsin column (Immobilized Pepsin, Pierce) at 15°C. The resulting peptides were captured on a BEH C18 Vanguard precolumn, separated by analytical chromatography (Acquity UPLC BEH C18, 1.7 µm 1.0 × 50 mm, Waters Corporation) using a 7–85%

acetonitrile gradient in 0.1% formic acid over 7.5 min, and electrosprayed into the Waters Synapt G2Si quadrupole time-of-flight mass spectrometer. The mass spectrometer was set to collect data in the Mobility, ESI+ mode; mass acquisition range of 200–2000 (m/z); scan time 0.4 s. Continuous lock mass correction was accomplished with infusion of leu-enkephalin (m/z = 556.277) every 30 s (mass accuracy of 1 ppm for calibration standard).

For peptide identification, the mass spectrometer was set to collect data in mobility-enhanced data-independent acquisition (MS^E), mobility ESI+ mode. Peptide masses were identified from triplicate analyses and data were analyzed using the ProteinLynx global server (PLGS) version 3.0 (Waters Corporation). Peptide masses were identified using a minimum number of 250 ion counts for low energy peptides and 50 ion counts for their fragment ions; the peptides also had to be larger than 1,500 Da. The following cutoffs were used to filter peptide sequence matches: minimum products per amino acid of 0.2, minimum score of 7, maximum MH+ error of 5 ppm, and a retention time RSD of 5%. In addition, the peptides had to be present in two of the three ID runs collected. The peptides identified in PLGS were then analyzed using DynamX 3.0 data analysis software (Waters Corporation). The relative deuterium uptake for each peptide was calculated by comparing the centroids of the mass envelopes of the deuterated samples with the undeuterated controls following previously published methods(Lumpkin and Komives 2019; Ramirez-Sarmiento and Komives 2018). For all HDX-MS data, 1 biological replicate was analyzed with 3 technical replicates. Data represented from different biological replicates are noted in their corresponding figures. All data are represented as mean values +/- SEM of 3 technical replicates due to limitations of processing software, however the LEAP robot provides highly reproducible data for biological replicates. The deuterium uptake was corrected for back-exchange using a global back exchange correction factor determined from the average percent exchange measured in disordered regions of each protein (Ramsey et al. 2017).

HDX-MS Data Analysis

The DynamX 3.0 (Waters) output of HDX-MS data for p52 and Bcl3 peptides (consolidated data in .csv format are provided as Supporting files) were processed using DECA version 1.16 (Lumpkin and Komives 2019; Ramirez-Sarmiento and Komives 2018) to calculate the fractional exchange compared to theoretical maximum at the residue level of individual peptides from individual states. The differences in fractional exchange of residues between pair of individual states were computed and plotted as a sequence ascribed heatmap using ‘R’. The ranges of the ‘difference in fractional exchange’ values were determined, and differences were represented as heatmaps of the blue-white-red color spectra to visualize the protection/deprotection. These ‘difference in fractional exchange’ values were also used to generate colored structural cartoons using the PyMOL Molecular Graphics System, Version 3.0 Schrödinger, LLC.

Author Contributions

V.Y.-F.W. and G.G. conceptualized and supervised the project. V.Y.-F.W. performed the HDX-MS experiments; T.B., S.S., and W.S. analyzed the HDX-MS data and generated the related figures. W.P. performed all the biochemistry and molecular biology experiments. D.Q. and A.V performed the EMSA. V.Y.-F.W., G.G. and T.B. wrote the paper with input from the other authors.

Acknowledgments

This work was supported by the Science and Technology Development Fund, Macao S.A.R. (FDCT) [project 0104/2019/A2 and 0089/2022/AFJ to V.Y.-F.W.]; the Multi-Year Research Grant from University of Macau [MYRG2018-00093-FHS to V.Y.-F.W.]; and the National Institutes of Health (NIH) [GM085490 G.G.].

Declaration of interests

GG and TB are cofounders of Siraj Therapeutics which has no relation to this project. The authors declare no competing interests.

Figure Legends

Figure 1. Phosphorylation of Bcl3 at S366 is critical for transcriptional activation by p52. (A, B) Structural organization of Bcl3 (the sequence numbering corresponds to UniProt ID P20749 lacking eight N-terminal residues) indicating ankyrin repeat domain (ARD) bounded by flexible N- and C-terminal regions; positions of serine residues undergoing phosphorylation investigated here are indicated in red. (C, D) Structural organization of p52 protomer (residues 1-398 of 900 from UniProt ID Q00653) observed in context of a dimer in association with a DNA-duplex; the residues at the boundaries of N-terminal domain (NTD), dimerization domain (DD), nuclear localization signal (NLS) and glycine rich region (GRR) boundaries are indicated. (E, F) Cartoons showing orthogonal views of predicted Bcl3, p52:p52 homodimer and DNA ternary complex; side view in (F) is showing only one protomer of p52 for clarity. (G) Luciferase reporter activity of a κB-promoter driven by co-expression of p52 and Bcl3. The S366A substitution of Bcl3 reduced the reporter activity while the S366E substitution enhanced it. The data were analyzed from three independent experiments performed in triplicate. RLU, relative luciferase unit. *$p<0.05$; **$p<0.01$; ***$p<0.001$ (t test). Error bars represent standard deviation (SD). (H) EMSA of κB-DNA with p52:p52 homodimer (expressed in *E. coli*) in absence or presence of Flag-tagged Bcl3 (expressed in HEK 293T cells, thus likely phosphorylated) respectively displaying formation of (p52:p52):DNA binary complex (lanes 2-3) and Bcl3:(p52:p52):DNA ternary complex (lanes 4-5). Expulsion of DNA from the (p52:p52):DNA binary complex by Bcl3-WT expressed in *E. coli* thus unphosphorylated (lanes 6-7). Formation of an unstable ternary complex by (p52:p52):DNA with Bcl3-3E$^{(S33/114/446E)}$ expressed in *E. coli* (lanes 8-10), and at a higher concentration Bcl3-3E competes with DNA for binding to p52:p52 homodimer dissolving the ternary complex (lane 8). Formation of a stabler ternary complex by (p52:p52):DNA with Bcl3-4E$^{(S33/114/366E446E)}$ expressed in *E. coli*, which is perturbed only weakly at a high concentration of Bcl3-4E (lanes 11-13). Absence of a ternary complex formation by (p52:p52):DNA with Bcl3-2E$^{(S33/114E)}$ expressed in *E. coli*, and corresponding lack of ability to displace DNA from (p52:p52):DNA by Bcl3-2E (lanes 14-16).

Figure 2. Dynamics of free Bcl3 protein. Deuterium uptake efficiencies of Bcl3-WT and Bcl3-4E as free proteins (A) mapped on their sequences at 0.5-, 1-, 2-, and 5-min timepoints; and (B) displayed on their structural models generated using experimentally determined structure of Bcl3-ARD and hypothetical extension of flexible regions at 5-min timepoint, respectively using Red to Green color spectra (Red indicates low exchange, and Green indicates high exchange). The N- and C-terminal domains of Bcl3 show higher exchange (reflecting flexibility) relative to the individual ankyrin repeats in the ARD domain (reflecting structural rigidity). Uptake plots of representative Bcl3-WT (grey) and Bcl3-4E (blue) peptides with (D) slow (residues 194-203), (E) intermediate (residues 117-149), and (F) fast (residues 388-413) exchanges, respectively. (G) Superposed uptake plots of a peptide (residues 9-45) displaying a contrasting difference in exchangeability between Bcl3-WT (low) and Bcl3-4E (high).

Figure 3. Dynamics of free p52 homodimer. A. Deuterium uptake efficiencies of free p52 (A) mapped on its sequence at 0.5-, 1-, 2-, and 5-min timepoints; and (B) displayed on its structural model of p52 homodimer adapted from experimentally determined structure of p52 and hypothetical extension of N- and C-terminal flexible regions at 5-min timepoint, respectively using Red to Green color spectra (Red-Low exchange, Green-High exchange). The protomers of p52 are colored identically based on average exchange of the two protomers in the homodimer; however, differential orientation and depth of the protomers in the 3D-projected view does not reflect this symmetry optimally. Uptake plots of representative p52 peptides with (C) slow (residues 66-84), (D) intermediate (resides 205-228), and (E) fast (residues 160-180) exchanges, respectively.

The difference in fractional uptake of deuterium in (A) Bcl3-4E vs. Bcl3-WT in their (p52:p52)-bound states, (B) Bcl3-WT in (p52:p52)-bound vs. unbound states; (C) Bcl3-4E in (p52:p52)-bound vs. unbound states; and (D) Bcl3-4E in (p52:p52):DNA-bound vs. (p52:p52)-bound states. The differences in fraction uptake displayed on Bcl3 structural model are shown on the left; sequence ascribed heatmaps are shown on the right. Changes are represented in Blue-White-Red spectra, with grey representing absence of data, blue signifies protection, and red signifies deprotection. Uptake plot panels of representative Bcl3 peptides (E) residues 9-45; (F) residues 120-149; (G) residues 136-149; (H) residues 183-193; (I) residues 263-283; (J) residues 306-319; and (K) residues 425-446 showing protective and deprotective effects of p52:p52 homodimer or (p52:p52):DNA on Bcl3-WT and Bcl3-4E.

Figure 5. **Dynamics changes of p52 homodimer upon binding to DNA and/or Bcl3-4E.** The difference in fractional uptake of deuterium in p52 homodimer (A) in DNA-bound vs. unbound states; (B) in Bcl3-4E-bound vs. unbound states; (C) in Bcl3-4E- and DNA-co-bound vs. Bcl3-4E-bound states; (D) in Bcl3-4E- and DNA-co-bound vs. DNA-bound states. The differences in fraction uptake displayed on p52 homodimer structural model are shown on the left; sequence ascribed heatmaps are shown on the right. Changes are represented in Blue-White-Red spectra, with grey representing absence of data, blue signifies protection, and red signifies deprotection. Uptake plot panels of representative p52 peptides (E) residues 41-53; and (F) residues 151-159 showing protective effect upon DNA binding. (G) Uptake plot panel of p52 peptide, residues 377-384, showing deprotective effect upon DNA binding. (H) Uptake plot panel of p52 peptide, residues 229-248, showing protective effect of upon both DNA and Bcl3-4E binding.

Figure 6. **Phosphorylation-mediated transcriptional regulatory switch of Bcl3.** (A) Sequence alignment of the βe-βf loop of NF-κB subunits. Secondary structures and connecting loops are drawn above the sequences. (B) Top: Streptavidin pulldown assay demonstrating the binding of p52-WT and -ADPS, -KDIN mutant proteins alone or together with His-Bcl3-4E to the biotinylated P-Selectin-κB DNA. Bottom: Plots showing the average amount of protein bound to DNA in three independent experiments at

the same condition. (C) Top: Luciferase reporter activity driven by co-expression of Bcl3 and p52 and its hybrid mutants indicates significant reduction in transcriptional activity with mutation. The data were analyzed from three independent experiments performed in triplicate. RLU, relative luciferase unit. **$p<0.01$; ***$p<0.001$ (t test). Error bars represent SD. Bottom: Western blot assay showing similar level of expression of p52 or its mutants in cells. (D) Top: Luciferase reporter activity driven by co-expression of p52 and Bcl3-WT or Bcl3-WT^{1-418} indicating enhanced transcriptional activation upon C-terminal truncation of Bcl3. Two equivalent clones of Bcl3-WT^{1-418} were tested. The data were analyzed from three independent experiments performed in triplicate. RLU, relative luciferase unit. *$p<0.05$; **$p<0.01$; ***$p<0.001$ (t test). Error bars represent SD. Bottom: Western blot assay showing similar level of expression of Bcl3-WT and Bcl3-WT^{1-418} in cells. (E) A cartoon of regulation of transcriptional activation by p52 through phosphorylation of Bcl3.

References

Basak, S., H. Kim, J. D. Kearns, V. Tergaonkar, E. O'Dea, S. L. Werner, C. A. Benedict, C. F. Ware, G. Ghosh, I. M. Verma, and A. Hoffmann. 2007. 'A fourth IkappaB protein within the NF-kappaB signaling module', *Cell*, 128: 369-81.

Bates, P. W., and S. Miyamoto. 2004. 'Expanded nuclear roles for IkappaBs', *Sci STKE*, 2004: pe48.

Bonilla, X., L. Parmentier, B. King, F. Bezrukov, G. Kaya, V. Zoete, V. B. Seplyarskiy, H. J. Sharpe, T. McKee, A. Letourneau, P. G. Ribaux, K. Popadin, N. Basset-Seguin, R. Ben Chaabene, F. A. Santoni, M. A. Andrianova, M. Guipponi, M. Garieri, C. Verdan, K. Grosdemange, O. Sumara, M. Eilers, I. Aifantis, O. Michielin, F. J. de Sauvage, S. E. Antonarakis, and S. I. Nikolaev. 2016. 'Genomic analysis identifies new drivers and progression pathways in skin basal cell carcinoma', *Nat Genet*, 48: 398-406.

Bours, V., G. Franzoso, V. Azarenko, S. Park, T. Kanno, K. Brown, and U. Siebenlist. 1993. 'The oncoprotein Bcl-3 directly transactivates through kappa B motifs via association with DNA-binding p50B homodimers', *Cell*, 72: 729-39.

Bundy, D. L., and T. W. McKeithan. 1997. 'Diverse effects of BCL3 phosphorylation on its modulation of NF-kappaB p52 homodimer binding to DNA', *J Biol Chem*, 272: 33132-9.

Cogswell, P. C., D. C. Guttridge, W. K. Funkhouser, and A. S. Baldwin, Jr. 2000. 'Selective activation of NF-kappa B subunits in human breast cancer: potential roles for NF-kappa B2/p52 and for Bcl-3', *Oncogene*, 19: 1123-31.

Cramer, P., C. J. Larson, G. L. Verdine, and C. W. Muller. 1997. 'Structure of the human NF-kappaB p52 homodimer-DNA complex at 2.1 A resolution', *EMBO J*, 16: 7078-90.

Dembinski, H. E., K. Wismer, J. D. Vargas, G. W. Suryawanshi, N. Kern, G. Kroon, H. J. Dyson, A. Hoffmann, and E. A. Komives. 2017. 'Functional importance of stripping in NFkappaB signaling revealed by a stripping-impaired IkappaBalpha mutant', *Proc Natl Acad Sci U S A*, 114: 1916-21.

Forbes, S. A., D. Beare, P. Gunasekaran, K. Leung, N. Bindal, H. Boutselakis, M. Ding, S. Bamford, C. Cole, S. Ward, C. Y. Kok, M. Jia, T. De, J. W. Teague, M. R. Stratton, U. McDermott, and P. J. Campbell. 2015. 'COSMIC: exploring the world's knowledge of somatic mutations in human cancer', *Nucleic Acids Res*, 43: D805-11.

Franzoso, G., L. Carlson, T. Scharton-Kersten, E. W. Shores, S. Epstein, A. Grinberg, T. Tran, E. Shacter, A. Leonardi, M. Anver, P. Love, A. Sher, and U. Siebenlist. 1997. 'Critical roles for the Bcl-3 oncoprotein in T cell-mediated immunity, splenic microarchitecture, and germinal center reactions', *Immunity*, 6: 479-90.

Fujita, T., G. P. Nolan, H. C. Liou, M. L. Scott, and D. Baltimore. 1993. 'The candidate proto-oncogene bcl-3 encodes a transcriptional coactivator that activates through NF-kappa B p50 homodimers', *Genes Dev*, 7: 1354-63.

Huxford, T., A. Hoffmann, and G. Ghosh. 2011. 'Understanding the logic of IkappaB:NF-kappaB regulation in structural terms', *Curr Top Microbiol Immunol*, 349: 1-24.

Huxford, T., D. B. Huang, S. Malek, and G. Ghosh. 1998. 'The crystal structure of the IkappaBalpha/NF-kappaB complex reveals mechanisms of NF-kappaB inactivation', *Cell*, 95: 759-70.

Inoue, J., T. Takahara, T. Akizawa, and O. Hino. 1993. 'Bcl-3, a member of the I kappa B proteins, has distinct specificity towards the Rel family of proteins', *Oncogene*, 8: 2067-73.

Keutgens, A., K. Shostak, P. Close, X. Zhang, B. Hennuy, M. Aussems, J. P. Chapelle, P. Viatour, A. Gothot, M. Fillet, and A. Chariot. 2010. 'The repressing function of the oncoprotein BCL-3 requires CtBP, while its polyubiquitination and degradation involve the E3 ligase TBLR1', *Mol Cell Biol*, 30: 4006-21.

Kohda, A., S. Yamazaki, and H. Sumimoto. 2016. 'The Nuclear Protein IkappaBzeta Forms a Transcriptionally Active Complex with Nuclear Factor-kappaB (NF-kappaB) p50 and the Lcn2 Promoter via the N- and C-terminal Ankyrin Repeat Motifs', *J Biol Chem*, 291: 20739-52.

Liu, H., L. Zeng, Y. Yang, Z. Huang, C. Guo, L. Huang, X. Niu, C. Zhang, and H. Wang. 2022. 'Bcl-3 regulates the function of Th17 cells through raptor mediated glycolysis metabolism', *Front Immunol*, 13: 929785.

Lumpkin, R. J., and E. A. Komives. 2019. 'DECA, A Comprehensive, Automatic Post-processing Program for HDX-MS Data', *Mol Cell Proteomics*, 18: 2516-23.

Maldonado, V., and J. Melendez-Zajgla. 2011. 'Role of Bcl-3 in solid tumors', *Mol Cancer*, 10: 152.
Mathas, S., K. Johrens, S. Joos, A. Lietz, F. Hummel, M. Janz, F. Jundt, I. Anagnostopoulos, K. Bommert, P. Lichter, H. Stein, C. Scheidereit, and B. Dorken. 2005. 'Elevated NF-kappaB p50 complex formation and Bcl-3 expression in classical Hodgkin, anaplastic large-cell, and other peripheral T-cell lymphomas', *Blood*, 106: 4287-93.
Narang, D., W. Chen, C. G. Ricci, and E. A. Komives. 2018. 'RelA-Containing NFkappaB Dimers Have Strikingly Different DNA-Binding Cavities in the Absence of DNA', *J Mol Biol*, 430: 1510-20.
Nishikori, M., Y. Maesako, C. Ueda, M. Kurata, T. Uchiyama, and H. Ohno. 2003. 'High-level expression of BCL3 differentiates t(2;5)(p23;q35)-positive anaplastic large cell lymphoma from Hodgkin disease', *Blood*, 101: 2789-96.
Nolan, G. P., T. Fujita, K. Bhatia, C. Huppi, H. C. Liou, M. L. Scott, and D. Baltimore. 1993. 'The bcl-3 proto-oncogene encodes a nuclear I kappa B-like molecule that preferentially interacts with NF-kappa B p50 and p52 in a phosphorylation-dependent manner', *Mol Cell Biol*, 13: 3557-66.
Oganesyan, I., C. Lento, and D. J. Wilson. 2018. 'Contemporary hydrogen deuterium exchange mass spectrometry', *Methods*, 144: 27-42.
Ohno, H., S. Doi, K. Yabumoto, S. Fukuhara, and T. W. McKeithan. 1993. 'Molecular characterization of the t(14;19)(q32;q13) translocation in chronic lymphocytic leukemia', *Leukemia*, 7: 2057-63.
Pan, W., L. Deng, H. Wang, and V. Y. Wang. 2022. 'Atypical IkappaB Bcl3 enhances the generation of the NF-kappaB p52 homodimer', *Front Cell Dev Biol*, 10: 930619.
Pan, W., V. A. Meshcheryakov, T. Li, Y. Wang, G. Ghosh, and V. Y. Wang. 2023. 'Structures of NF-kappaB p52 homodimer-DNA complexes rationalize binding mechanisms and transcription activation', *Elife*, 12.
Phelps, C. B., L. L. Sengchanthalangsy, T. Huxford, and G. Ghosh. 2000. 'Mechanism of I kappa B alpha binding to NF-kappa B dimers', *J Biol Chem*, 275: 29840-6.
Ramirez-Sarmiento, C. A., and E. A. Komives. 2018. 'Hydrogen-deuterium exchange mass spectrometry reveals folding and allostery in protein-protein interactions', *Methods*.
Ramsey, K. M., H. E. Dembinski, W. Chen, C. G. Ricci, and E. A. Komives. 2017. 'DNA and IkappaBalpha Both Induce Long-Range Conformational Changes in NFkappaB', *J Mol Biol*, 429: 999-1008.
Schwarz, E. M., P. Krimpenfort, A. Berns, and I. M. Verma. 1997. 'Immunological defects in mice with a targeted disruption in Bcl-3', *Genes Dev*, 11: 187-97.
Trinh, D. V., N. Zhu, G. Farhang, B. J. Kim, and T. Huxford. 2008. 'The nuclear I kappaB protein I kappaB zeta specifically binds NF-kappaB p50 homodimers and forms a ternary complex on kappaB DNA', *J Mol Biol*, 379: 122-35.
Vinciauskaite, V., and G. R. Masson. 2022. 'Fundamentals of HDX-MS', *Essays Biochem*.
Wang, V. Y., W. Huang, M. Asagiri, N. Spann, A. Hoffmann, C. Glass, and G. Ghosh. 2012. 'The transcriptional specificity of NF-kappaB dimers is coded within the kappaB DNA response elements', *Cell Rep*, 2: 824-39.
Wang, V. Y., Y. Li, D. Kim, X. Zhong, Q. Du, M. Ghassemian, and G. Ghosh. 2017. 'Bcl3 Phosphorylation by Akt, Erk2, and IKK Is Required for Its Transcriptional Activity', *Mol Cell*, 67: 484-97 e5.
Westerheide, S. D., M. W. Mayo, V. Anest, J. L. Hanson, and A. S. Baldwin, Jr. 2001. 'The putative oncoprotein Bcl-3 induces cyclin D1 to stimulate G(1) transition', *Mol Cell Biol*, 21: 8428-36.
Yamamoto, M., S. Yamazaki, S. Uematsu, S. Sato, H. Hemmi, K. Hoshino, T. Kaisho, H. Kuwata, O. Takeuchi, K. Takeshige, T. Saitoh, S. Yamaoka, N. Yamamoto, S. Yamamoto, T. Muta, K. Takeda, and S. Akira. 2004. 'Regulation of Toll/IL-1-receptor-mediated gene expression by the inducible nuclear protein IkappaBzeta', *Nature*, 430: 218-22.
Yuan, W., Z. Zhang, B. Dai, Q. Wei, J. Liu, Y. Liu, Y. Liu, L. He, and D. Zhou. 2016. 'Whole-exome sequencing of duodenal adenocarcinoma identifies recurrent Wnt/beta-catenin signaling pathway mutations', *Cancer*, 122: 1689-96.

Main Figures

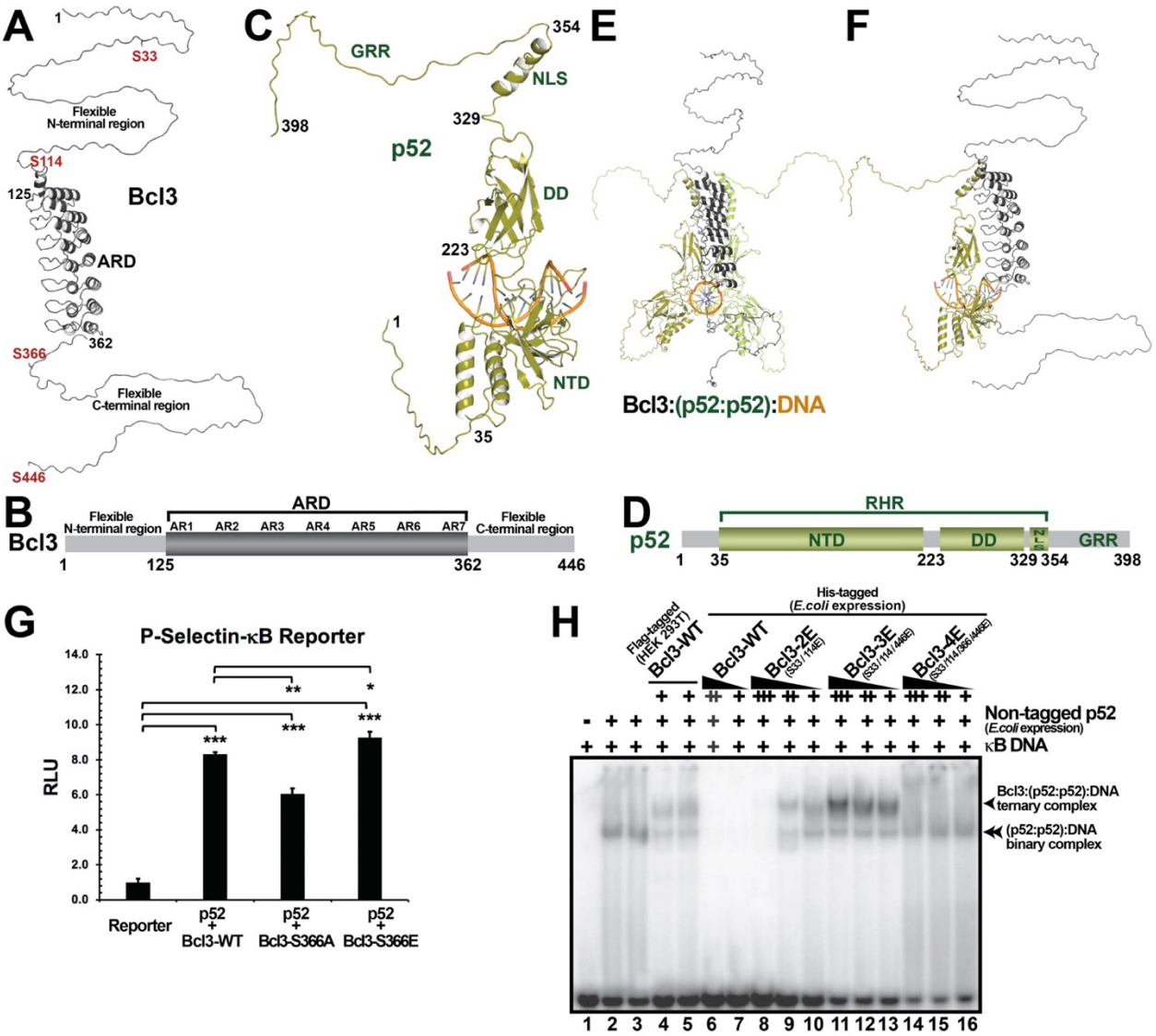

Figure 1

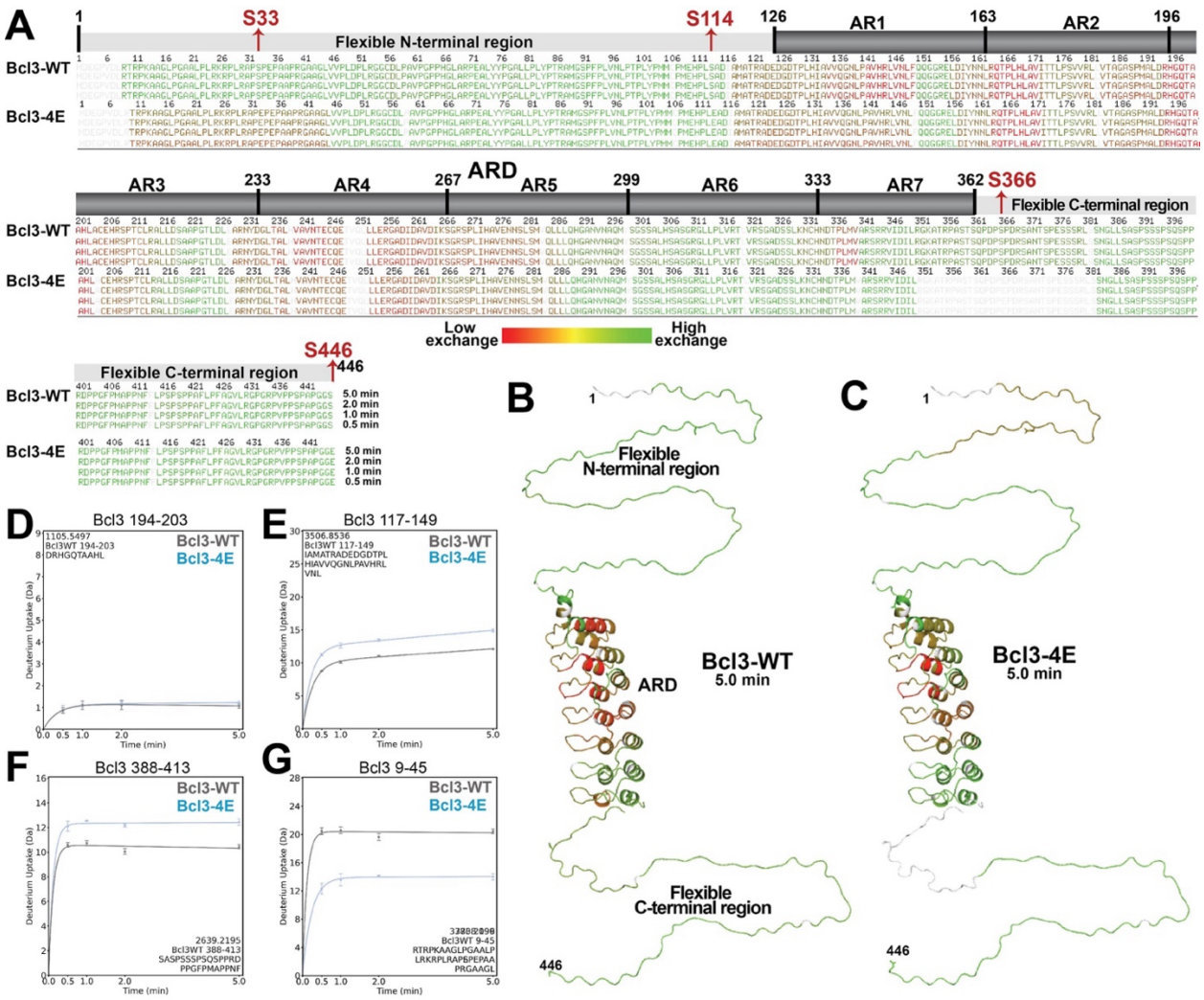
A
S33
S114
Flexible N-terminal region
AR1
AR2
AR3
AR4
AR5
AR6
AR7
ARD
S366
Flexible C-terminal region
Bcl3-WT
Bcl3-4E
Low exchange
High exchange
S446
Flexible C-terminal region
5.0 min
2.0 min
1.0 min
0.5 min
B
C
Flexible N-terminal region
ARD
Bcl3-WT 5.0 min
Bcl3-4E 5.0 min
Flexible C-terminal region
D
Bcl3 194-203
E
Bcl3 117-149
F
Bcl3 388-413
G
Bcl3 9-45
Deuterium Uptake (Da)
Time (min)

Figure 2

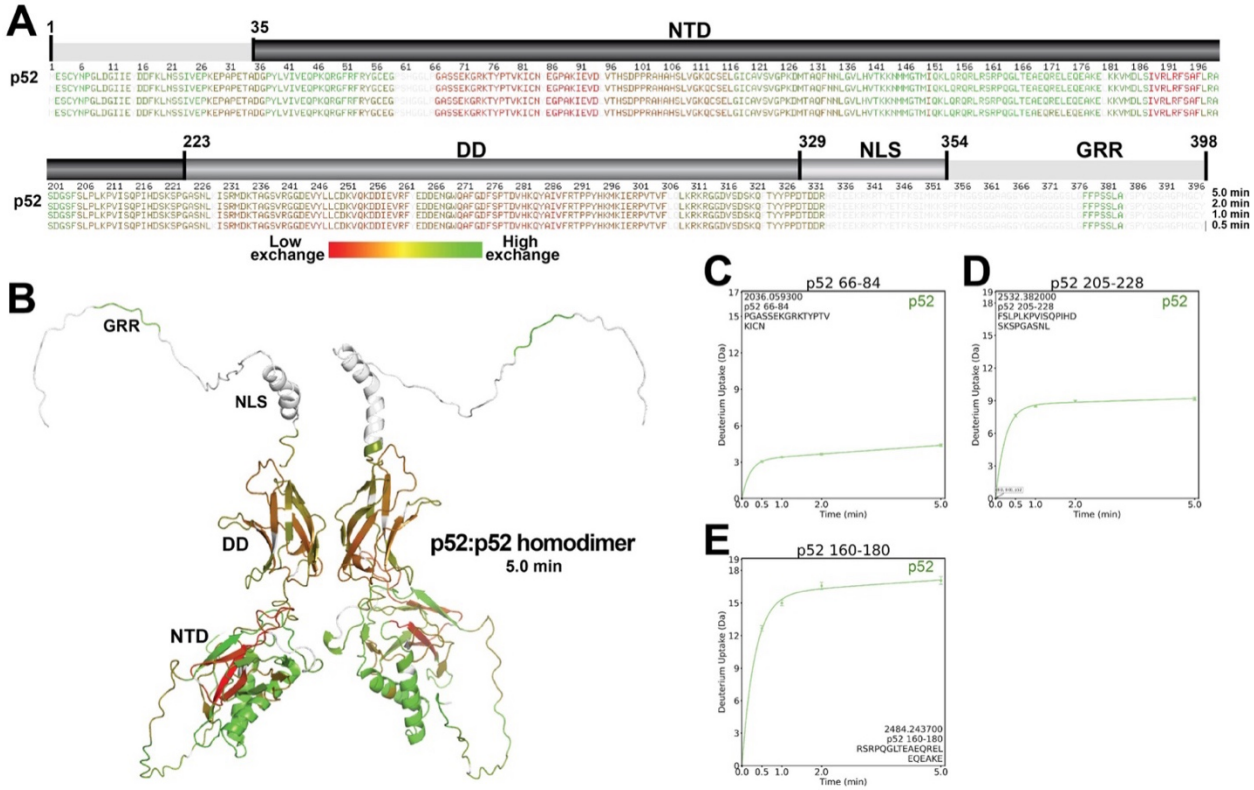
A
1
35
NTD
p52
223
DD
329
NLS
354
GRR
398
5.0 min
2.0 min
1.0 min
0.5 min
Low exchange
High exchange
B
GRR
NLS
DD
NTD
p52:p52 homodimer
5.0 min
C
p52 66-84
2036.059300
p52 66-84
PGASSEKGRKTYPTV
KICN
p52
Deuterium Uptake (Da)
Time (min)
D
p52 205-228
2532.382000
p52 205-228
FSLPLKPVISQPIHD
SKSPGASNL
p52
Deuterium Uptake (Da)
Time (min)
E
p52 160-180
p52
2484.243700
p52 160-180
RSRPQGLTEAEQREL
EQEAKE
Deuterium Uptake (Da)
Time (min)

Figure 3

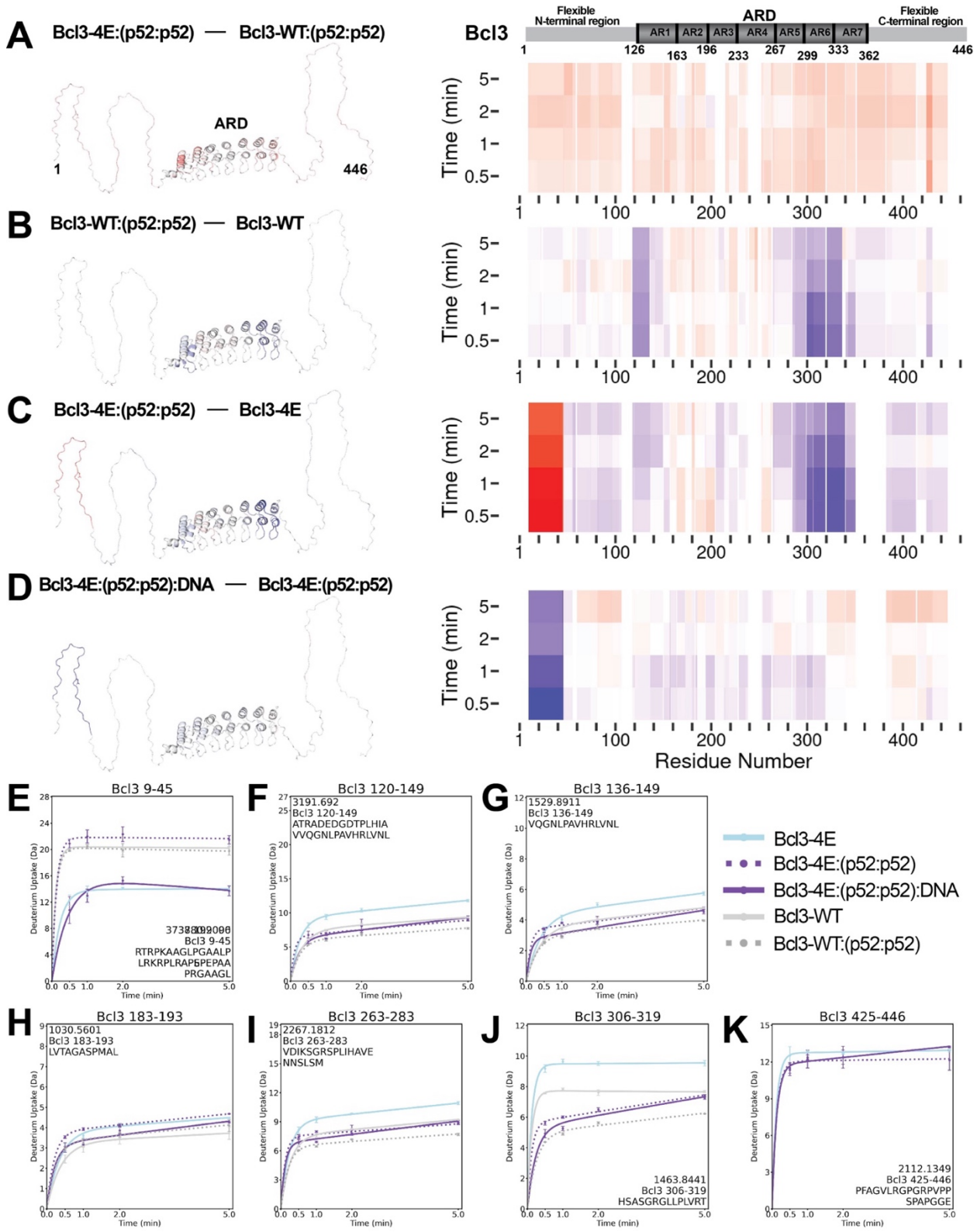
A
Bcl3-4E:(p52:p52) — Bcl3-WT:(p52:p52)
ARD
1
446
B
Bcl3-WT:(p52:p52) — Bcl3-WT
C
Bcl3-4E:(p52:p52) — Bcl3-4E
D
Bcl3-4E:(p52:p52):DNA — Bcl3-4E:(p52:p52)
Bcl3
Flexible N-terminal region
ARD
Flexible C-terminal region
AR1
AR2
AR3
AR4
AR5
AR6
AR7
1
126
163
196
233
267
299
333
362
446
Time (min)
Residue Number
E
Bcl3 9-45
F
Bcl3 120-149
3191.692
Bcl3 120-149
ATRADEDGDTPLHIA
VVQGNLPAVHRLVNL
G
Bcl3 136-149
1529.8911
Bcl3 136-149
VQGNLPAVHRLVNL
Bcl3-4E
Bcl3-4E:(p52:p52)
Bcl3-4E:(p52:p52):DNA
Bcl3-WT
Bcl3-WT:(p52:p52)
H
Bcl3 183-193
1030.5601
Bcl3 183-193
LVTAGASPMAL
I
Bcl3 263-283
2267.1812
Bcl3 263-283
VDIKSGRSPLIHAVE
NNSLSM
J
Bcl3 306-319
1463.8441
Bcl3 306-319
HSASGRGLLPLVRT
K
Bcl3 425-446
2112.1349
Bcl3 425-446
PFAGVLRGPGRPVPP
SPAPGGE
Deuterium Uptake (Da)
Time (min)

Figure 4

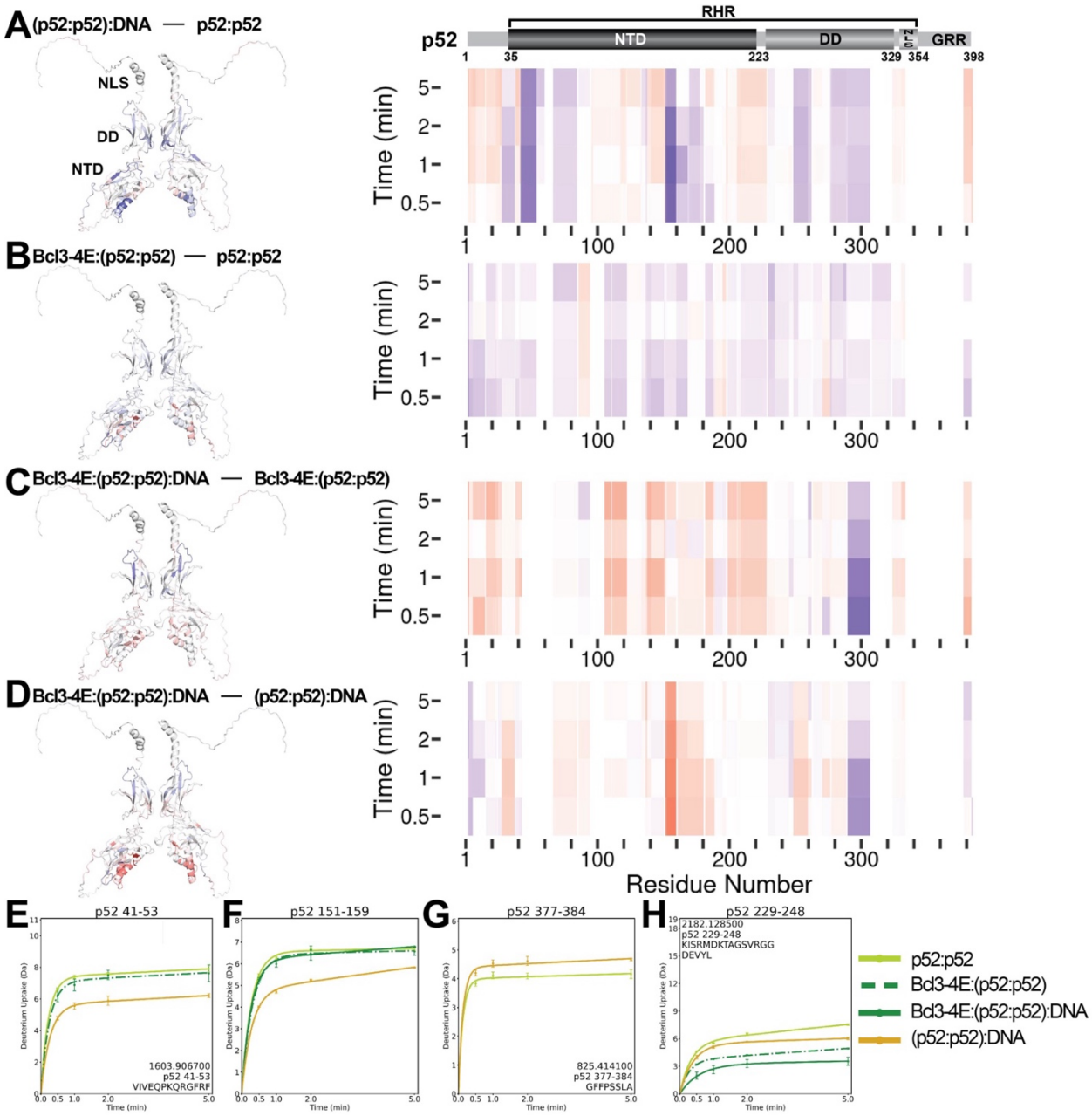
A (p52:p52):DNA — p52:p52
NLS
DD
NTD
RHR
p52
NTD
DD
GRR
1
35
223
329
354
398
Time (min)
5
2
1
0.5
1
100
200
300
B Bcl3-4E:(p52:p52) — p52:p52
C Bcl3-4E:(p52:p52):DNA — Bcl3-4E:(p52:p52)
D Bcl3-4E:(p52:p52):DNA — (p52:p52):DNA
Residue Number
E p52 41-53
1603.906700
p52 41-53
VIVEQPKQRGFRF
F p52 151-159
G p52 377-384
825.414100
p52 377-384
GFFPSSLA
H p52 229-248
2182.128500
p52 229-248
KISRMDKTAGSVRGG
DEVYL
Deuterium Uptake (Da)
Time (min)
p52:p52
Bd3-4E:(p52:p52)
Bd3-4E:(p52:p52):DNA
(p52:p52):DNA

Figure 5

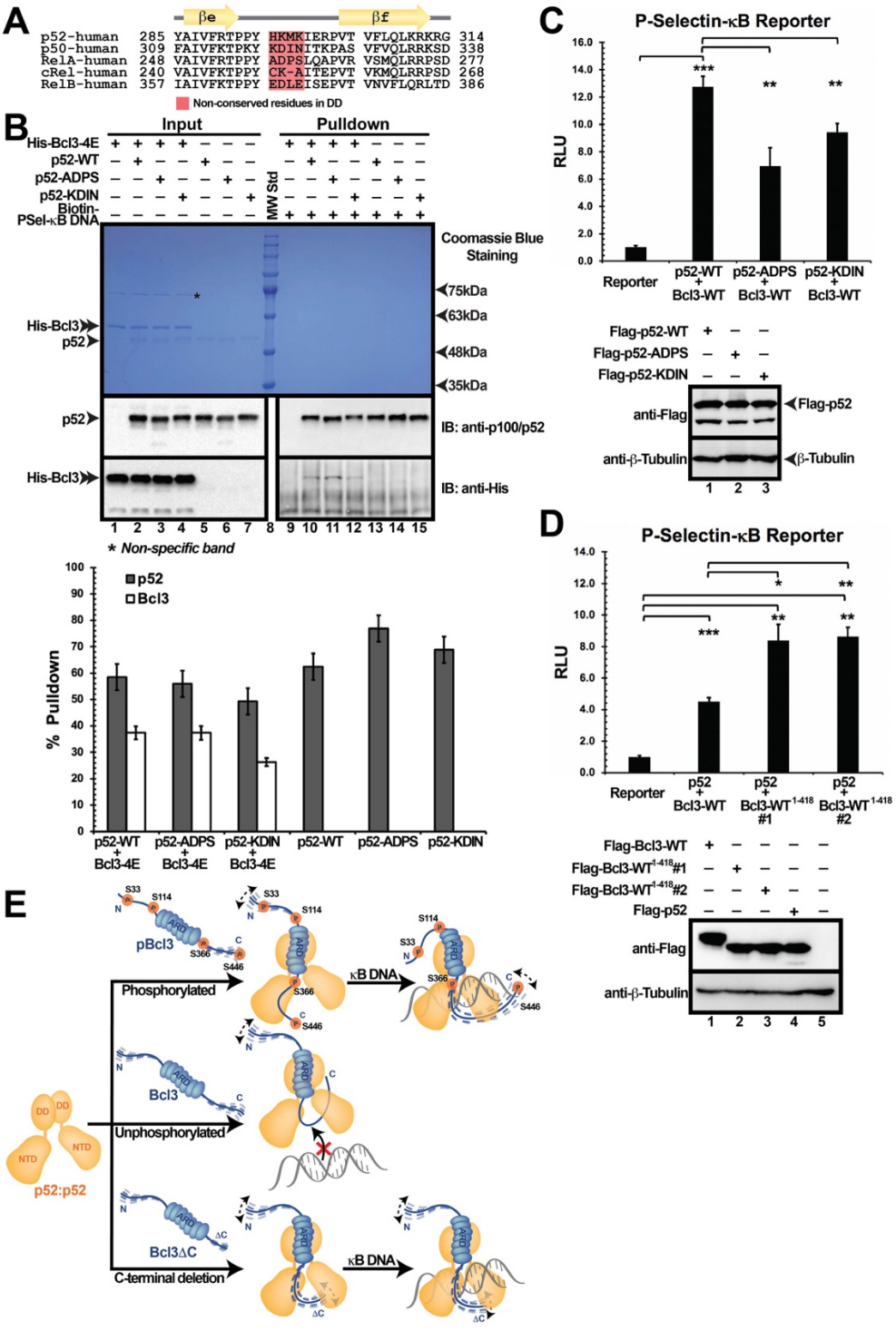
A
βe
βf
p52-human 285 YAIVFRTPPY HKMKIERPVT VFLQLKRKRG 314
p50-human 309 FAIVFKTPKY KDINITKPAS VFVQLRRKSD 338
RelA-human 248 VAIVFRTPPY ADPSLQAPVR VSMQLRRPSD 277
cRel-human 240 VAIVFKTPPY CK-AITEPVT VKMQLRRPSD 268
RelB-human 357 IAIVFKTPPY EDLEISEPVT VNVFLQRLTD 386
Non-conserved residues in DD
B
Input
Pulldown
His-Bcl3-4E
p52-WT
p52-ADPS
p52-KDIN
Biotin-PSel-κB DNA
MW Std
Coomassie Blue Staining
75kDa
63kDa
48kDa
35kDa
His-Bcl3
p52
IB: anti-p100/p52
IB: anti-His
* Non-specific band
p52
Bcl3
% Pulldown
p52-WT + Bcl3-4E
p52-ADPS + Bcl3-4E
p52-KDIN + Bcl3-4E
p52-WT
p52-ADPS
p52-KDIN
C
P-Selectin-κB Reporter
RLU
Reporter
p52-WT + Bcl3-WT
p52-ADPS + Bcl3-WT
p52-KDIN + Bcl3-WT
Flag-p52-WT
Flag-p52-ADPS
Flag-p52-KDIN
anti-Flag
Flag-p52
anti-β-Tubulin
β-Tubulin
D
P-Selectin-κB Reporter
RLU
Reporter
p52 + Bcl3-WT
p52 + Bcl3-WT1-418 #1
p52 + Bcl3-WT1-418 #2
Flag-Bcl3-WT
Flag-Bcl3-WT1-418#1
Flag-Bcl3-WT1-418#2
Flag-p52
anti-Flag
anti-β-Tubulin
E
pBcl3
Phosphorylated
κB DNA
Bcl3
Unphosphorylated
p52:p52
Bcl3ΔC
C-terminal deletion
κB DNA

Figure 6